Appl. Phys. B 53, 101–107 (1991)

Applied Physics B Photophysics and Laser Chemistry

Discharge Ignition Phenomena in CO_2 and N_2O Lasers with Preliminary Filling of the Interelectrode Gap by Electrons

R. E. Beverly III

R. E. Beverly III and Associates, 854 Pipestone Drive, Worthington, OH 43235, USA

Received 28 March 1991/ Accepted 16 May 1991

Abstract. A comprehensive model is presented that describes preionization and discharge ignition processes in large-aperture molecular-gas lasers. By initially filling the interelectrode gap with electrons and establishing a space-charge screen at the cathode, electron avalanche begins adjacent to the anode. Cathode-directed ionization waves develop and ignite the discharge. Dynamic profiling of the electric-field distribution and Penning ionization of a readily ionizable additive combine to decrease both the ignition and quasi-steady-state voltages.

PACS: 42.55 Em, 52.80 Hc, 52.35 – g

Development of CO_2 lasers using VUV preionization has been impeded because of discharge instabilities that occur in devices with large transverse gaps and large volumes. Realization of volumetrically uniform preionization is extremely difficult when the gap dimension greatly exceeds the mean free path for VUV photons. Contoured electrodes with profiles of extreme accuracy are needed to minimize field distortions and ensure discharge stability. Furthermore, fast (low-inductance) circuitry is necessary to rapidly increase the electron concentration from photopreionization levels ($n_{e0} \sim 10^6$–$10^8\,cm^{-3}$) to lasing densities ($n_e \sim 10^{12}$–$10^{14}\,cm^{-3}$). The minimum voltage needed to initiate a stable, volumetric self-sustained discharge (VSD) U_{min} is quite high when the transverse gap g is increased beyond a few centimeters, even for mixtures with a low molecular-gas content K (e.g., $U_{min} \cong 280\,kV$ for $g = 30\,cm$ and $K = 20\%$). U_{min} can be reduced by addition of small concentrations of readily ionizable organic compounds that contribute electrons to the discharge via VUV photoionization and via Penning reactions with electronically excited N_2 molecules. The two most common additives are tri-*n*-propylamine (TPA, 7.23 eV ionization potential) and triethylamine (TEA, 7.59 eV ionization potential). For a constant specific input energy ξ_i, however, any reduction in the quasi-steady self-sustained voltage U_{qs} will require an *arc-free* increase in the quasi-steady-state duration t_{qs}. Furthermore, the optimum partial pressure for the Penning process ($P_{ri} \cong 1$–1.5 Torr) is greater than that required for enhanced VUV photoionization, thus reducing the density of photoelectrons at large distances from the radiation source to values less than in the pure gas.

Alternatively, an auxiliary discharge [1–15], placed adjacent to an unprofiled (i.e., flat) cathode with marginally radiused edges, acts as an electron beam capable of producing in-depth volume preionization levels which are greater than the minimum required for discharge stability. The auxiliary discharge can be implemented as a volume discharge, a barrier discharge, a corona discharge, or a complete or incomplete surface discharge. One major advantage of this technique over VUV irradiation is that it is able to efficiently preionize large-aperture devices that contain a high percentage of molecular gas. With the subsequent application of a tailored voltage pulse to the main transverse gap, space-charge screening effects reduce field enhancement at the cathode thereby retarding or suppressing instabilities from developing within cathode spots associated with the boundary layer. Simple, easily machined electrodes can therefore be used without danger of arcing at the edges. Dynamic enhancement of the electric field at or near the anode during the preionization phase reduces the minimum voltage to $U_{min} \cong (2/3)U_{sb}$, where U_{sb} is the static self-breakdown voltage. With these electrode geometries, U_{sb} is about half the value measured with profiled electrodes having a uniform field distribution. Recent advancement of this technology has led to impressive aperture ($g \geqq 70\,cm$) and volume ($V = 400\,l$) scaling [16, 17].

1. Necessary Conditions for Preionization and Field Enhancement

To provide complete, in-depth preionization of the transverse gap, it is necessary that the auxiliary discharge flux be maintained for a duration t_{aux} which approximates or exceeds the characteristic electron drift time across the main gap, i.e.,

$$t_{aux} \geqq t_{dr} = \frac{g}{\mu_e E_0}, \tag{1}$$

where

$$E_0 = \frac{U_{bias}}{g} \approx \frac{U_{sb}}{3g} \tag{2}$$

is the quasi-dc field applied to the main transverse gap prior to discharge ignition. U_{bias} is the bias voltage and μ_e is the electron mobility. If, on the other hand, a slowly rising voltage pulse is used both for preliminary filling of the gap with preionization electrons and ignition of the discharge, then

$$E_0 \approx \frac{2U_{pk}}{3g}, \tag{3}$$

where U_{pk} is the peak discharge voltage. The auxiliary discharge is electrically driven for a duration t_{ad} and, typically, $t_{ad} \approx t_{aux}$. Furthermore, it is necessary that the current density extracted from the auxiliary discharge J_{aux} exceed a minimum value to effect space-charge screening of the cathode, i.e.,

$$J_{aux} \geqq J_{min} = f\left(\text{gas composition}, P, \frac{dU_d}{dt}\right), \tag{4}$$

where P is the total gas pressure and dU_d/dt is the rate of rise of the voltage applied to the main transverse gap. The duration t_{aux}, effective electrode area A, and current density J_{aux} define the total charge q_{aux} transferred between cathode and anode during the preionization phase.

2. Discharge Preionization and Ignition Model

Numerical modeling and simulation of discharge ignition have been performed by Beverly [18, 19] and Baitsur and Firsov [10]. The former model, which includes negative ions, is followed here. The conservation equations for charged particle densities $n(x,t)$ in one spatial dimension are

$$\frac{\partial n_e}{\partial t} = S_e - \frac{\partial J_e}{\partial x}, \tag{5}$$

$$\frac{\partial n_+}{\partial t} = S_+ - \frac{\partial J_+}{\partial x}, \tag{6}$$

$$\frac{\partial n_-}{\partial t} = S_- - \frac{\partial J_-}{\partial x}, \tag{7}$$

where n represents particle concentration (particles/cm^3), S collectively represents source and loss terms (particles/cm^3 · s) associated with various kinetic processes, J represents scalar current density (particles/cm^2 · s), and the subscripts e, +, and − denote electrons, positive ions, and negative ions, respectively. The relations between particle current density J, drift velocity W (cm/s), and mobility μ (cm^2/V · s) are

$$J_e(x,t) = n_e W_e = -\mu_e n_e E, \tag{8}$$

$$J_+(x,t) = n_+ W_+ = \mu_+ n_+ E, \tag{9}$$

$$J_-(x,t) = n_- W_- = -\mu_- n_- E, \tag{10}$$

where the electric field vector points in a direction from anode ($x = g$) to cathode ($x = 0$) and, thus, $E = |\vec{E}| < 0$. With this sign convention, W_e and W_- are positive and W_+ is negative. The source terms are

$$S_e(x,t) = (\bar{k}_i - \bar{k}_a) n_e N - k_r^{ei} n_e n_+ + \bar{k}_d n_- N + S_{vuv} + S_P, \tag{11}$$

$$S_+(x,t) = \bar{k}_i n_e N - k_r^{ei} n_e n_+ - k_r^{ii} n_+ n_- + S_{vuv} + S_P, \tag{12}$$

$$S_-(x,t) = \bar{k}_a n_e N - \bar{k}_d n_- N - k_r^{ii} n_+ n_-, \tag{13}$$

where processes (and rate coefficients) include primary electron-impact ionization (k_i), electron attachment (k_a), electron detachment (k_d), electron-ion recombination (k_r^{ei}), and ion-ion recombination (k_r^{ii}). The bar notation indicates rate coefficients which are weighted for the particular gas mixture and which are functions of the local value of the reduced field E/N, where N is the total particle concentration. S_P and S_{vuv} are additional source terms, described subsequently, for Penning ionization of a readily ionizable organic additive and for VUV preionization by an external illumination source. Equations (5–7) must be solved simultaneously with Poisson's equation relating the electric field $E(x,t)$ to the charge density $\varrho(x,t)$,

$$\frac{\partial E}{\partial x} = -\frac{\varrho}{\varepsilon}, \tag{14}$$

$$\varrho = e(n_+ - n_e - n_-), \tag{15}$$

where ε is the permittivity of free space and e is the electronic charge.

The charged particle conservation equations are subject to mixed Dirichlet and Neumann boundary conditions at the electrodes. At the cathode,

$$\phi_e(0,t) = 6.24 \times 10^{15} J_{aux}, \tag{16}$$

$$n_-(0,t) = 0, \tag{17}$$

where ϕ_e is the electron flux (electrons/cm^2 · s) and J_{aux} is the beam current density from the auxiliary discharge (mA/cm^2). At the anode,

$$n_+(g,t) = 0. \tag{18}$$

The constant of integration is lost in solving (14) and thus the additional condition

$$U_d(t) = -\int_0^g E(x,t)\,dx \tag{19}$$

is imposed where U_d is the voltage between the electrodes. U_d can be incorporated into Kirchoff's equation, with appropriate RLC terms, to model the external capacitive-discharge circuit (a discussion of circuit response is given in [20]). For the present model, however, the discharge is

simply connected to a voltage source whose temporal characteristics are (Fig. 1):

$$U_d(t)=\begin{cases} U_{bias}, & t\leqq t_{bias} \\ U_{pk}+\dfrac{(U_{pk}-U_{bias})}{2}\left\{1-\cos\left[\dfrac{\pi(t-t_{bias})}{t_r}\right]\right\}, & t_{bias}<t<t_{bias}+2t_r \\ 0, & t\geqq t_{bias}+2t_r. \end{cases} \quad (20)$$

A formula for the discharge current has been derived from first principles [21], from which we determine the current density:

$$J_d(t)=\frac{e}{g}\int_0^g (n_+W_+ - n_-W_- - n_eW_e)dx. \quad (21)$$

The equation describing evolution of the combined $N_2\ a'^1\Sigma_u$ ($\tau_r \geqq 23$ ms) and $a^1\Pi_g$ ($\tau_r = 80$ μs) metastable state concentration $n_m(x,t)$ is

$$\frac{\partial n_m}{\partial t}=k_m n_e[N_2]-\frac{n_m}{\bar{\tau}}, \quad (22)$$

where k_m is the rate coefficient for electronic excitation from the N_2 ground state to the metastable level, $\bar{\tau}$ is the characteristic time for collisional deactivation of the metastable level (weighted for the particular gas mixture), and $[N_2]$ is the nitrogen gas concentration (constant). Losses due to radiative decay (τ_r) are ignored. Although the $N_2\ A^3\Sigma_u^+$ and $B^3\Pi_g$ states are produced in significant quantities in CO_2-laser discharges, only the *a*-states have sufficient energy ($\cong 8.5$ eV) and are produced in large enough concentrations to participate in Penning ionization of typical readily ionizable compounds. The source term for Penning ionization is therefore

$$S_P(x,t)=\frac{n_m}{\tau_P}, \quad (23)$$

where τ_P is the characteristic time for Penning collisions ($1/\tau_P = k_P N_{ri}$, where N_{ri} is the concentration of readily ionizable molecules).

Certain types of auxiliary discharges also emit VUV radiation. The source term for VUV preionization through a mesh cathode is

$$S_{vuv}(x,t)=\begin{cases} \zeta\alpha\phi_{vuv}\exp(-\alpha x)(t/t_1), & t\leqq t_1 \\ \zeta\alpha\phi_{vuv}\exp(-\alpha x)\exp(-t/t_2), & t>t_1, \end{cases} \quad (24)$$

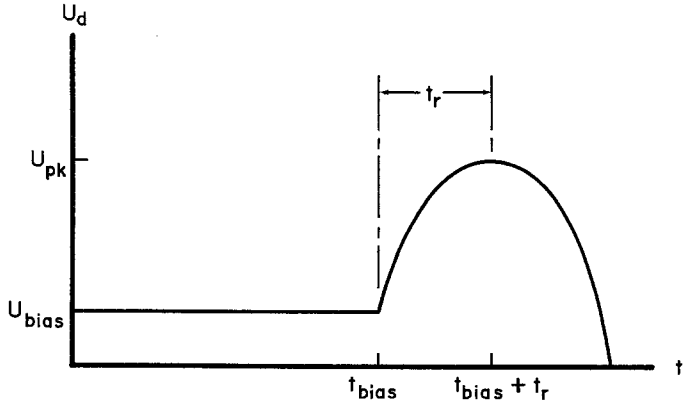

Fig. 1. Voltage waveform for the discharge ignition model

where $\alpha = \sigma_a N_{ri}$ is the photoabsorption coefficient (cm^{-1}), σ_a is the photoabsorption cross section (cm^2), ζ is the photoionization yield (dimensionless), and ϕ_{vuv} is the peak photon flux (photons/$cm^2 \cdot s$) incident upon the gas volume through the mesh cathode structure. The temporal dependence of the VUV irradiation is thus described by a linear rise over a duration t_1 followed by an exponential decay with time constant t_2. An analogous, optional source term is included for VUV preionization through the anode; firing of these sources can be delayed until $t' = t - t_d$.

3. Method of Solution and Rate Data

Solution of the hyperbolic equations (5–7) is accomplished using the low-phase-error phoenical sharp and smooth transport algorithm (LPE SHASTA) as originally proposed by Zalesak [22] and implemented by Morrow et al. [23–26]. To impose the Neumann boundary condition (16), ϕ_e is simply added to the corrected anti-diffusive flux at the cathode. Dirichlet boundary conditions are specified by (17) and (18). Source terms were integrated using a time-splitting technique [27]. Integration of (14) is performed separately and accuracy is greatly improved by subdividing each spatial interval into a finer mesh. The charge density distribution on the fine mesh is evaluated by a fourth-order (cubic) Lagrangian interpolator, using only the central interval for accuracy. Solution of (22) is effected by transforming the single parabolic partial differential equation (PDE) into a coupled set of ordinary differential equations (ODEs), one ODE for each spatial mesh point (*method of lines*). Since this set of ODEs is not stiff, solution is obtained using a straightforward, fourth-order Runge-Kutta algorithm. Two fictitious mesh points are introduced beyond the boundaries as a method for continuing the solution into the electrodes. This technique avoids problems associated with reducing numerical order when approaching a boundary.

Rate coefficients for CO_2:N_2:He gas mixtures were computed by solution of Boltzmann's transport equation using the ELENDIF code [28] and included 39 inelastic processes. Computed rate coefficients are shown in Fig. 2 for a gas mixture with high molecular-gas content ($K = 0.50$). Here, 1 Td $\equiv$ 1 Townsend $= 10^{-17}$ V · cm^2. The predicted self-sustained equilibrium can be estimated by finding the value of E/N at which $\bar{k}_i = \bar{k}_a$; for a 1:4:5 mixture, this occurs at $E_{qs}/N = 49$ Td without a readily ionizable additive, while for a 4:16:80 mixture, the corresponding value is lower ($E_{qs}/N = 28$ Td), consistent with a lower fractional content of molecular gases. The

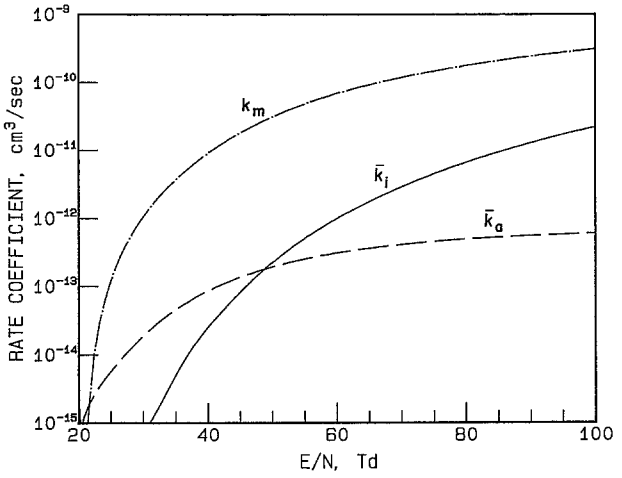

Fig. 2. Rate coefficients for a CO_2:N_2:He=1:4:5 gas mixture at 300 K

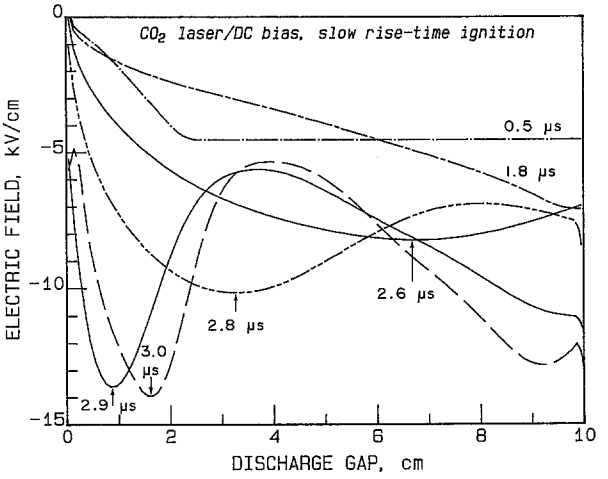

Fig. 4. Computed E-field during preionization and ignition of a CO_2-laser gas mixture; each arrow locates the crest of the cathode-directed ionization wave at a particular instant

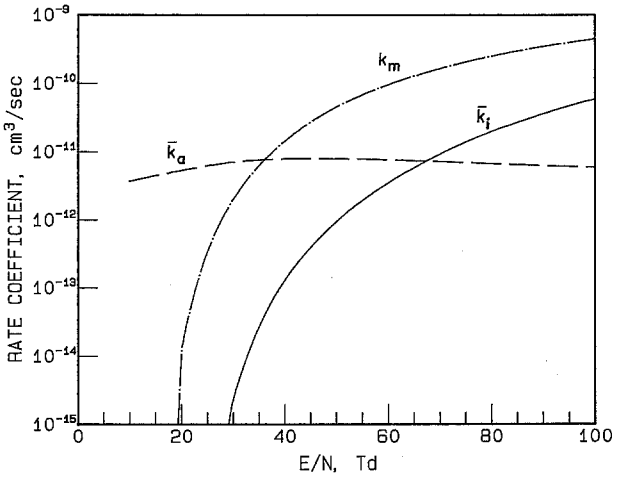

Fig. 3. Rate coefficients for an N_2O:CO:N_2:He=3:10:10:47 gas mixture at 300 K

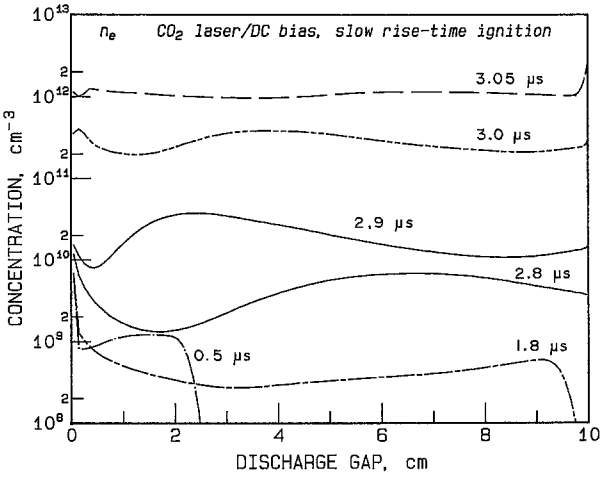

Fig. 5. n_e evolution corresponding to Fig. 4

parameterized electron drift velocity is

$$|W_e| = c\left(\frac{|E|}{N}\right)^m, \tag{25}$$

where $c=2.44\times10^{17}$, $m=0.68$ (CO_2:N_2:He=1:4:5) and $c=6.11\times10^{18}$, $m=0.77$ (CO_2:N_2:He=4:16:80). Similarly, rate coefficients were also computed for a representative N_2O-laser gas mixture as shown in Fig. 3. The predicted quasi-steady reduced field is $E_{qs}/N=67$ Td, which does not include the effects of electron detachment as discussed subsequently. The added electron production rate due to detachment reactions will reduce E_{qs}/N substantially. Electron drift velocity coefficients for the N_2O:CO:N_2:He=3:10:10:47 gas mixture are $c=4.80\times10^{17}$ and $m=0.70$.

Sources of fundamental data are as follows: τ_P and τ [29, 30], σ_a and ζ [31, 32], $k_r^{ei}(E/N)$ [33], and k_r^{ii} and k_d [34]. Penning rate data are only available for TPA. Positive and negative ion mobilities in pure gases can be found in [35, 36]. Blanc's law is then used to calculate ionic mobility in the various gas mixtures [37].

4. Discharge Ignition Phenomena

4.1 CO_2 Lasers

The computational run shown here is for a CO_2:N_2:He =1:4:5 gas mixture ($T=293$ K, $P=750$ Torr) which contained an admixture of TPA ($P_{ri}=1.5$ Torr). The interelectrode gap is $g=10$ cm. Cathode and anode VUV preionization are absent. The discharge initiation scheme is described by auxiliary preionization in the presence of a quasi-dc field followed by application of a slow-ignition voltage pulse ($t_{bias}=1.8$ μs, $t_r=2$ μs, $J_{aux}=1$ mA/cm², U_{bias} =40 kV, and $U_{pk}=120$ kV). During the *filling* phase ($t\leqq t_{bias}$), the electron preionization front progresses in the absence of electron-impact ionization and no positive charge carriers are generated (Figs. 4 and 5). The electron flux reaches $x\cong2.4$ cm at $t=0.5$ μs and almost reaches the anode at $t=1.8$ μs; the negative space charge present at the conclusion of the filling phase distorts the field so that it is largest at the anode ($E=7.1$ kV/cm). In the absence of this space charge, the electric field would be uniform across the gap and equal to 4.0 kV/cm. As $U_d(t)$ increases,

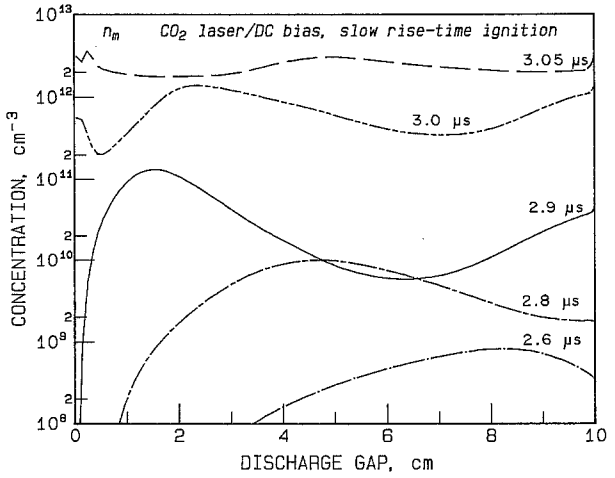

Fig. 6. n_m evolution corresponding to Fig. 4

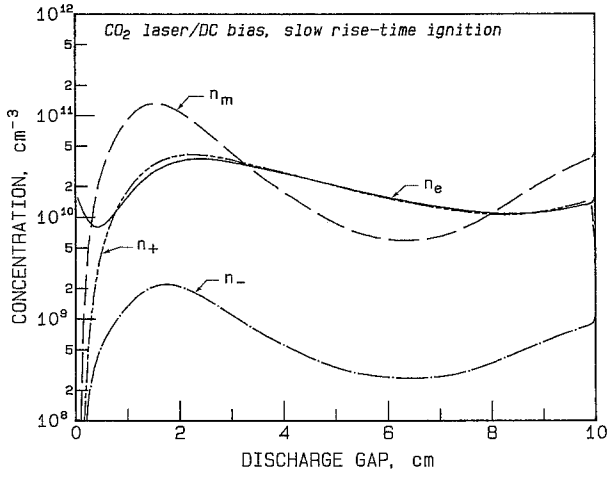

Fig. 7. Species concentrations at $t = 2.9\,\mu s$ for the CO_2-laser discharge

electron avalanche begins within the local region of highest field strength. A cathode-directed ionization wave with a velocity $\sim 10^7$ cm/s develops near the anode at $t \cong 2.5\,\mu s$, accelerates, and reaches the cathode at $t \approx 2.95\,\mu s$. After passage of the first cathode-directed wave, the region of maximum plasma conductivity is adjacent to the cathode and the maximum electric field again occurs near the anode, launching a second ionization wave just prior to discharge ignition (curve labelled $t = 3.0\,\mu s$). These waves then relax and establish a homogeneous VSD at $E_{qs} = U_{qs}/g$, which is typically 20% smaller than the value predicted in Sect. 3 by neglecting Penning ionization. Additionally, the presence of these waves decreases the minimum ignition field E_{min} by ≈ 30–40%.

Evolution of the N_2 metastable concentration with time is shown in Fig. 6. n_m is initially largest at the anode and the peak value follows the spatio-temporal evolution of the electric field more closely than n_e. Lastly, spatially dependent concentrations of all species at the time corresponding to imminent arrival of the first ionization wave at the cathode are shown in Fig. 7. Note that for the present conditions, the concentration of negative ions has little influence upon discharge development. This situation is misleading, since gas impurities (e.g., O_2, H_2O) and secondary reaction by-products (CO, NO_x) typically found in recirculating-flow systems have not been included in this computation. Additional computational studies show that a high concentration of NO_x, for example, impedes transport of the electron beam and greatly alters the discharge ignition mechanism. Negative ions become the principal negative charge carrier and establishment of a stable VSD is unlikely.

Identical computer runs have been performed with the addition of VUV preionization through a mesh anode structure, consisting of a fast rise-time ($t_1 = 100$ ns), exponential-decay ($t_2 = 750$ ns) source that produces an in-band (~ 160 nm) VUV photon energy density of $0.2\,\mu J/cm^2$. If the VUV source is fired during the rise in discharge voltage ($t_d \approx t_{bias} + t_r/2$), then sufficient positive space charge is generated adjacent to the anode to shift the peak electric field and, hence, the origin for the cathode-directed ionization wave into the mid-gap region. Because the duration of the VUV source is characteristically less than the discharge voltage rise time, anode space-charge screening does not persist throughout the ignition period. Simultaneous cathode- and anode-directed waves form and dissipate prior to realization of quasi-equilibrium conditions.

4.2 N_2O Lasers

Advancement of N_2O lasers has been frustrated by the highly electronegative nature of representative gas mixtures. The threshold energy for the dissociative attachment reaction

$$N_2O + e^- \rightarrow N_2 + O^- \tag{26}$$

is very low ($E_{thr} \cong 0.15$ eV) and the weighted rate coefficient is quite large ($\bar{k}_a \sim 10^{-11}$ cm^3/s) over a wide range ($E/N = 10$–100 Td). This forces the discharge to operate at high E_{qs}/N values in self-sustained devices (cf. Fig. 3), which is non-optimal both for excitation of the upper laser level and for retarding instabilities. These instabilities induce striations that degrade discharge homogeneity and severely limit the specific input and output energies. Furthermore, operation of an auxiliary discharge in this environment is not possible since the electron flux would be immediately depleted even for very small E_0.

Electron losses due to dissociative attachment can be offset by electron detachment involving the principal negative ion and added CO gas:

$$O^- + CO \rightarrow CO_2 + e^-, \tag{27}$$

where $k_d = 5.5 \times 10^{-10}$ cm^3/s. The electron attachment and detachment frequencies approximately balance when the ratio of molecular gases $[CO]/[N_2O] \approx 4$. Significant improvements in laser output energy, specific input and output energies, and discharge efficiency have been reported using the auxiliary-discharge technique [38].

Numerical simulations were performed for an N_2O:CO:N_2:He = 3:10:10:47 gas mixture ($T = 293$ K, $P = 450$ Torr) which contained an admixture of TPA ($P_{ri} = 0.9$ Torr). The interelectrode gap is $g = 10$ cm. Cathode

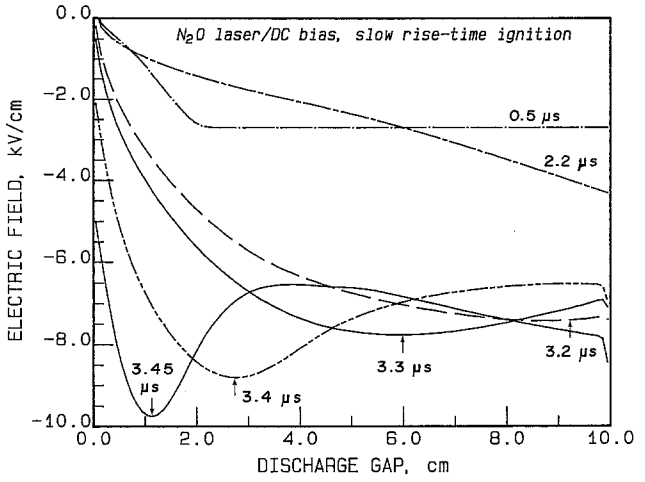

Fig. 8. Computed E-field during preionization and ignition of an N_2O-laser gas mixture

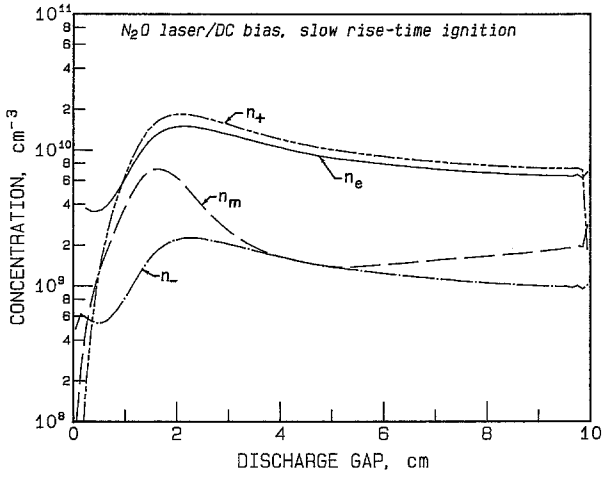

Fig. 9. Species concentrations at $t=3.45\,\mu s$ for the N_2O-laser discharge

and anode VUV preionization are absent. The discharge initiation scheme is described by auxiliary preionization in the presence of a quasi-dc field followed by application of a slow-ignition voltage pulse ($t_{bias}=2.2\,\mu s$, $t_r=2\,\mu s$, $J_{aux}=1\,mA/cm^2$, $U_{bias}=24\,kV$, and $U_{pk}=96\,kV$). Progress of the auxiliary-discharge electron flux can be tracked in Fig. 8, which shows the computed electric-field distribution for selected times. The electron flux reaches $x\cong 2\,cm$ at $t=0.5\,\mu s$ and the anode at $t=2.2\,\mu s$. Negative space charge present at the end of the filling phase distorts the field so that it is largest at the anode ($E=4.2\,kV/cm$). In the absence of this space charge, the electric field would be uniform across the gap and equal to 2.4 kV/cm. A cathode-directed ionization wave develops near the anode at $t\approx 3.2\,\mu s$, accelerates, and reaches the cathode at $t\approx 3.5\,\mu s$, i.e., before the peak discharge voltage is reached. This phenomenon is completely analogous to that observed experimentally and computationally with CO_2 lasers employing auxiliary-discharge preionization, although the E-field amplitude of the ionization wave is typically not as large.

The spatially-dependent concentrations of all species at the time corresponding to imminent arrival of the ionization wave at the cathode are shown in Fig. 9. The negative-ion concentration is larger than observed with typical CO_2-laser simulations, but still only about one-tenth of the electron concentration. Thus, the presence of CO largely compensates for the strongly-attaching nature of the N_2O component. The metastable N_2 concentration, however, is greatly reduced. Ignition simulations in typical CO_2-laser discharges yield $n_m \geqq 10^{11}\,cm^{-3}$ at the crest of the ionization wave while the peak value here is $n_m=7\times 10^9\,cm^{-3}$. Hence, strong quenching by N_2O reduces the metastable concentration to levels which are insignificant and Penning ionization of the readily ionizable additive is ineffective. This is confirmed by experiments where these compounds had no effect on either U_{min} or U_{qs} in self-sustained N_2O-laser gas mixtures [38].

The importance of electron detachment via reaction (27) is demonstrated by an additional simulation with $\bar{k}_d=0$. Negative ions immediately become the principal negative charge carrier and the preionization front stalls adjacent to the cathode. Even a dramatic increase in U_{bias} was unable to transport these negative ions across the gap in a reasonable time ($t\sim t_{bias}$) since $\mu_- \ll \mu_e$. Therefore, the processes of preliminary filling of the discharge gap with an electron flux from an auxiliary discharge, dynamic profiling of the E-field distribution, and ignition via ionization waves are only possible in N_2O lasers with optimized gas mixtures.

5. Discussion and Conclusions

The processes of preliminary filling of the discharge gap with electrons, dynamic profiling of the electric field, discharge ignition, and establishment of a VSD occur under conditions of greatly reduced cathode field and absence of the usual cathode fall layer. Electrons are continuously supplied by the auxiliary discharge and an electron flux flows through the cathode boundary layer. To obtain maximum benefit from the dynamic profiling process, it is important that the gap be completely filled with preionization electrons, viz., the electron flux must reach the anode prior to electron avalanche and discharge ignition. The requirements for a minimum preionization concentration and for complete filling of the gap, however, are necessary although insufficient conditions for formation of ionization waves. Although the location of the field maximum will occur at the anode for any value of $E_0 \ll E_{sb}$, a cathode-directed ionization wave will not form if E_0 is too small regardless of whether or not the gap is completely filled with preionization electrons. To ensure optimal efficacy of discharge ignition utilizing the dynamic profiling phenomenon, E_0 should be adjusted so that $E(g, t_{dr})$ is just below the threshold for ionization avalanche. ($E_0 \approx E_{sb}/3$ is usually satisfactory). This requirement is also necessary to remain in a regime where losses due to dissociative attachment are negligible. The low-current, low-energy electron beam extracted from the auxiliary discharge can therefore progress across the discharge gap unimpeded.

Only cathode-directed waves are possible if the gap is completely filled with electrons during the preionization

phase. If incomplete filling occurs, or if a VUV source at the anode is fired during the rise in applied voltage [5], both cathode- and anode-directed waves are formed. These model predictions agree well with observations of ionization-wave behavior made using an image-converter camera [8, 10]. The combination of ionization waves and Penning ionization involving metastable species reduces the ignition voltage by 30–40% compared with fast-pulse, VUV-preionized discharges. The presence of readily ionizable additives also decreases the quasi-steady discharge voltage and promotes discharge stability by reducing the growth rate for the multistep-ionization instability [12].

Complete depletion of electrons from the cathode region and accumulation of a large positive space charge in the cathode boundary layer are prevented by continued preionization during the ignition process. For auxiliary barrier discharge sources ($J_{aux} \leqq 1\,mA/cm^2$), maintenance of the negative space-charge screen requires a rate of voltage rise $dU_d/dt < 10\,kV/\mu s$ [10]. *Higher-productivity* auxiliary surface discharges [13] can relax this requirement ($dU_d/dt \leqq 30$–$40\,kV/\mu s$) and are especially significant in large-aperture systems. By shifting the region of ionization avalanche into the mid-gap, mid-electrode region, distortions and perturbations to the electric field within the boundary layers have minimal impact upon volumetric discharge stability, which permits the use of unprofiled electrodes.

References

1. V.V. Apollonov, Yu.M. Vas'kovskii, M.I. Zhavoronkov, A.M. Prokhorov, R.E. Rovinskii, V.E. Rogalin, N.D. Ustinov, K.N. Firsov, I.S. Tsenina, V.A. Yamshchikov: Sov. J. Quantum Electron. **15**, 1–3 (1985)
2. V.V. Apollonov, N. Akhunov, G.G. Baitsur, K.N. Firsov, A.M. Prokhorov, V.R. Minenkov, B.V. Semkin, B.G. Shubin, A.V. Yushin, V.A. Yamshchikov: Proc. Intern. Conf. on LASERS '85 (Las Vegas, Nevada 1985) pp. 681–687
3. V.V. Apollonov, G.G. Baitsur, A.M. Prokhorov, K.N. Firsov: Sov. Tech. Phys. Lett. **11**, 521–523 (1985)
4. V.V. Apollonov, G.G. Baitsur, A.M. Prokhorov, K.N. Firsov: Sov. J. Quantum Electron. **16**, 1680–1682 (1986)
5. V.V. Apollonov, G.G. Baitsur, A.M. Prokhorov, K.N. Firsov: Sov. J. Quantum Electron. **16**, 1294–1295 (1986)
6. V.V. Apollonov, G.G. Baitsur, A.M. Prokhorov, K.N. Firsov: Sov. J. Quantum Electron. **17**, 76–82 (1987)
7. V.V. Apollonov, G.G. Baitsur, V.R. Minenkov, A.M. Prokhorov, B.V. Semkin, K.N. Firsov, B.G. Shubin, A.V. Yushin: Sov. J. Quantum Electron. **17**, 134–135 (1987)
8. V.V. Apollonov, G.G. Baitsur, A.M. Prokhorov, K.N. Firsov: Sov. Tech. Phys. Lett. **13**, 230–231 (1987)
9. V.V. Apollonov, G.G. Baitsur, B.B. Kudabaev, A.M. Prokhorov, B.V. Semkin, K.N. Trefilov, B.G. Shubin: Sov. J. Quantum Electron. **17**, 1364–1365 (1987)
10. G.G. Baitsur, K.N. Firsov: Dynamic profiling of the electric field at the stage of formation of the volumetric self-sustained discharge – research and analysis of methods and capabilities, General Physics Institute, Moscow, Preprint No. 260 (1987) (in Russian)
11. V.V. Apollonov, G.G. Baitsur, I.G. Kononov, K.N. Firsov, V.A. Yamshchikov: Sov. J. Quantum Electron. **18**, 321–325 (1988)
12. V.V. Apollonov, G.G. Baitsur, A.M. Prokhorov, S.K. Semenov, K.N. Firsov: Sov. J. Quantum Electron. **18**, 351–354 (1988)
13. V.V. Apollonov, G.G. Baitsur, A.M. Prokhorov, E.E. Trefilov, K.N. Firsov, B.G. Shubin: Sov. Tech. Phys. Lett. **14**, 241–242 (1988)
14. V.V. Apollonov, G.G. Baitsur, B.B. Kudabaev, V.R. Minenkov, A.M. Prokhorov, B.V. Semkin, K.N. Firsov, B.G. Shubin: Instrum. Exp. Technol. **32**, 149–152 (1989)
15. V.V. Apollonov, G.G. Baitsur, O.B. Koval'chuk, V.N. Konev, V.R. Minenkov, K.N. Firsov, B.G. Shubin: Sov. Tech. Phys. Lett. **14**, 915–916 (1988)
16. V.V. Apollonov, G.G. Baitsur, K.N. Firsov, O.B. Koval'chuk, V.R. Minenkov, B.G. Shubin: Ultraviolet-preionized volume self-sustained discharge in a volume of 400 liters, paper scheduled for presentation at Pulse Power for Lasers III (Los Angeles 1991); Proc. SPIE **1411** (to be published)
17. G.G. Baitsur, V.V. Apollonov, K.N. Firsov, V.R. Minenkov, B.G. Shubin: New principles and techniques of volume self-sustained discharge formation in high-power molecular lasers, paper scheduled for presentation at Pulse Power for Lasers III (Los Angeles 1991); Proc. SPIE **1411** (to be published)
18. R.E. Beverly III: Modeling of ignition phenomena in transverse discharges preionized by an auxiliary discharge, Proc. XIII Intern. Conf. on Coherent and Nonlinear Optics (Minsk, BSSR 1988) Vol. IV, pp. 29–30
19. R.E. Beverly III: Enhanced transverse discharge stability using preionization from an auxiliary barrier discharge, Seventh Intern. Symp. on Gas Flow and Chemical Lasers (Wien 1988); Proc SPIE **1031**, 458–466 (1989)
20. R.E. Beverly III: Pulsed power modeling of very-large-aperture, transverse-discharge CO_2 Lasers. Appl. Phys. B **53** (1991)
21. N. Sato: J. Phys. D **13**, L 3–L 6 (1980)
22. S.T. Zalesak: J. Comput. Phys. **31**, 335–362 (1979)
23. R. Morrow: J. Comput. Phys. **43**, 1–15 (1981)
24. R. Morrow, L.E. Cram: J. Comput. Phys. **57**, 129–136 (1985)
25. P. Steinle, R. Morrow: J. Comput. Phys. **80**, 61–71 (1989)
26. P. Steinle, R. Morrow, A.I. Roberts: J. Comput. Phys. **85**, 493–499 (1989)
27. R. Morrow: J. Comput. Phys. **46**, 454–461 (1982)
28. W.L. Morgan, B.M. Penetrante: Computer Phys. Commun. **58**, 127–152 (1990)
29. V.V. Apollonov, N. Akhunov, S.I. Derzhavin, I.G. Kononov, K.N. Firsov, Yu.A. Shakir, V.A. Yamshchikov: Sov. Tech. Phys. Lett. **6**, 450–452 (1980)
30. L.G. Piper: J. Chem. Phys. **87**, 1625–1629 (1987)
31. D.F. Grosjean, P. Bletzinger: IEEE J. QE-**13**, 898–904 (1977)
32. A. Goehlich, W. Terbeck, H.F. Dobele: Rev. Sci. Instrum. **58**, 701–703 (1987)
33. I.M. Littlewood, M.C. Cornell, K.J. Nygaard: J. Chem. Phys. **81**, 1264–1270 (1984)
34. R.E. Beverly III: Opt. Quantum Electron. **14**, 501–513 (1982)
35. H.W. Ellis, R.Y. Pai, E.W. McDaniel, E.A. Mason, L. Viehland: At. Data Nucl. Data Tables **17**, 177–210 (1976)
36. H.W. Ellis, E.W. McDaniel, D.L. Albritton, L.A. Viehland, S. Lin, E.A. Mason: At. Data Nucl. Data Tables **22**, 179–217 (1978)
37. E.W. McDaniel, E.A. Mason: *The Mobility and Diffusion of Ions in Gases* (Wiley, New York 1973) p. 159
38. V.V. Apollonov, G.G. Baitsur, I.G. Kononov, A.M. Prokhorov, S.K. Semenov, K.N. Firsov, V.A. Yamshchikov: Sov. J. Quantum Electron. **19**, 839–840 (1989)